

ORIGINAL ARTICLE

Antimicrobial Effect and Cytocompatibility After Using Different Decontamination Methods on Titanium Implant Surfaces: An In Vitro Study

Andrea Alonso-Español¹  | Enrique Bravo¹ | Ana Carrillo de Albornoz¹  | María Martínez¹ | Katharina Doll-Nikutta^{2,3} | Andreas Winkel^{2,3}  | Meike Stiesch^{2,3} | David Herrera¹  | Bettina Alonso¹ | Mariano Sanz¹

¹Etiology and Therapy of Periodontal and Periimplant Diseases (ETEP) Research Group, Faculty of Dentistry, Complutense University, Madrid, Spain | ²Department of Prosthetic Dentistry and Biomedical Materials Science, Hannover Medical School, Hannover, Germany | ³Lower Saxony Center for Biomedical Engineering, Implant Research and Development (NIFE), Hannover, Germany

Correspondence: Mariano Sanz (marsan@ucm.es)

Received: 9 October 2024 | **Revised:** 24 December 2024 | **Accepted:** 14 January 2025

Funding: This study was funded by the ETEP Research Group (*Cátedra Extraordinaria Dentaid e Investigación Periodontal*), by SEPA Foundation (*Beca de Investigación Sepa 2023—Estudios diseñados en el marco de la investigación básica, preclínica y clínica—Aula de Investigación SEPA 2023*), and by Complutense University of Madrid (UCM) (*Programa de Erasmus + en Prácticas (SMT) para alumnos salientes (OUT) del Doctorado en Ciencias Odontológicas UCM*). Besides, it was also funded by Deutsche Forschungsgemeinschaft (DFG, German Research Foundation) under the Collaborative Research Center SFB/TRR-298-SIIRI—Project ID 426335750.

Keywords: 3D peri-implant model | curcumin | decontamination | electrolytic decontamination | multispecies biofilm | xanthohumol

ABSTRACT

Aim: To evaluate in vitro the antibacterial efficacy and cytocompatibility of different implant-decontamination methods, using both 2D and 3D peri-implant mucosa models.

Methods: Four decontamination methods [chlorhexidine (CHX), electrolytic treatment (GS), curcumin (CUR), xanthohumol (XN)] were compared in four independent experiments, three with a 2D peri-implant mucosa model on titanium surfaces and another on a 3D peri-implant mucosa model. These decontamination procedures were tested for their antibacterial effect using a multispecies biofilm model with *Streptococcus oralis*, *Actinomyces naeslundii*, *Veillonella dispar*, and *Porphyromonas gingivalis* for 24 h. Direct cytocompatibility evaluating the impact of the treatments on tissue cells as well as indirect cytocompatibility (colonization of treated implant surfaces by tissue cells) were also tested. Both outcomes were assessed by confocal laser scanning microscopy supported by neural networks.

Results: CHX demonstrated a strong alteration of cytocompatibility and antibacterial effect, but did not remove biofilm biomass. XN and CUR demonstrated antibacterial effect and biofilm removal action, as well as cytocompatibility. GS showed antibacterial capacity with a combination of areas completely clean of biofilm with others in which a non-vital biofilm remained. In the 3D peri-implant mucosa model, XN and CUR showed maintenance of the mucosa integrity after treatment, whereas CHX and GS displayed disruption in the mucosal layers.

Conclusions: Phytotherapeutics (CUR and XN) were the most cytocompatible substances and showed the largest antimicrobial effect. GS displayed antibiofilm activity with a localized “bubble-shaped effect” and impaired tissue cell morphology and integrity, compromising cytocompatibility, and CHX showed antimicrobial capacity, without reducing biofilm biomass and with altered cytocompatibility.

1 | Introduction

Peri-implantitis is a chronic inflammatory disease of the hard and soft peri-implant tissues triggered by bacterial colonization and biofilm formation on the implant and implant component surfaces. Its treatment is based on arresting the inflammation by eliminating or removing the biofilm deposits (surface decontamination). However, the achievement of the disease resolution with these methods is currently not highly predictable (Berglundh et al. 2019).

The arrest of the peri-implant tissue inflammation depends on a thorough decontamination of the implant surface and the prevention of subsequent bacterial re-colonization. However, the complexity of the subgingival microbiome associated with peri-implantitis (Charalampakis and Belibasakis 2015; Padiál-Molina et al. 2016; Rakic, Grusovin, and Canullo 2016) and the challenges associated with the limited access to contaminated areas (Sanz-Martin et al. 2021; Steiger-Ronay et al. 2017) represent relevant difficulties in this process.

Various implant surface decontamination approaches, such as mechanical/physical (de Tapia et al. 2019), use of laser/photodynamic devices (Ramanauskaite et al. 2023), locally delivered antimicrobials (Al-Hashedi et al. 2016; Machtei et al. 2021), systemically delivered antimicrobials (Carrillo de Albornoz et al. 2024), probiotics (Gennai et al. 2023), and different chemical agents (Dommsich et al. 2023; Wilensky et al. 2023), have been proposed and evaluated independently or in combination with submarginal peri-implant tissue instrumentation (Renvert and Polyzois 2018). However, their efficacy in arresting peri-implantitis has been shown to be heterogeneous and inconclusive (Cosgarea et al. 2023). The recently published clinical practice guideline for the treatment of peri-implant diseases emphasizes the need for further research in these interventions, especially randomized clinical trials (Herrera et al. 2023). However, before evaluating their efficacy using well-designed clinical research, innovative or alternative decontamination protocols must be carefully tested using validated *in vitro* models to determine their potential antimicrobial effect, and at the same time, their safety, assuring that there is no harm to implant surfaces and surrounding tissues (Al-Hashedi et al. 2016; Hakki et al. 2017; Luengo et al. 2022; Sahrman et al. 2021; Sanz-Martin et al. 2021).

One of the recently proposed alternative approaches, the use of electrolytic decontamination methods (Bosshardt et al. 2022), is based on the application of low-voltage electrical currents to decontaminate the implant surfaces. Although the results from *in vitro* studies are encouraging regarding biofilm removal (Virto et al. 2023), there is limited evidence on its cytocompatibility (Kotsakis et al. 2016; Ungvari et al. 2010; Wheelis et al. 2016). Recently, a device based on this electrochemical concept has been made commercially available for the treatment of peri-implantitis (GalvoSurge, Institut Straumann AG, Basel, Switzerland).

Similarly, natural vegetal-based extracts, such as curcumin (CUR) and xanthohumol (XN), have been tested *in vitro* for their antimicrobial properties against potential pathogenic bacterial species. A recent report from our research group using a dynamic multispecies biofilm model, has reported a significant antimicrobial effect when applied on contaminated dental implant

surfaces (Alonso-Espanol et al. 2023). However, the cytocompatibility of these applications has not been addressed. In fact, a recent *in vitro* study evaluating the efficacy of different commercialized chemical agents used as implant decontaminants, cautioned against their potential cytotoxicity (Stein et al. 2023).

It was, therefore, the aim of the presented *in vitro* investigation to evaluate the potential antimicrobial and biofilm reduction effect, as well as their cytocompatibility of three innovative implant-decontamination methods, when applied on titanium surfaces.

2 | Methods

Four independent *in vitro* experiments were designed and conducted, three using a 2D peri-implant mucosa model on titanium surfaces and another using a 3D peri-implant mucosa model. No ethics approval was required due to the *in vitro* nature of the study.

To understand how the decontamination treatments affect both on the biofilm formed on the implant surfaces and on the subsequent recolonization of the surface by tissue cells, the 2D peri-implant mucosa model was used. The rationale for this method was that both the biofilm contamination and the implant surface may be affected by the proposed treatments, what may have a subsequent impact on tissue healing. However, to study the direct interaction between the treatments and both the formed biofilms and the peri-implant tissues, the 3D peri-implant mucosa model was used. The hypothesis was based on the assumption that antimicrobial treatments as chlorhexidine (CHX) or the electrolytic treatment (GS) would demonstrate an antimicrobial effect but a concomitant significant impact on cell viability, while the phytochemical treatments of XN and CUR would demonstrate a similar antimicrobial effect with significantly lesser cytotoxicity.

2.1 | Experiment Designs Using the 2D Model

Three independent experiments were carried out at the Center for Biomedical Engineering, Implant Research and Development (NIFE) in Hannover, Germany.

Experiment 1 (Figure 1, Exp. 1) aimed to assess the antimicrobial effect of the proposed decontamination protocols, while experiment 2 (Figure 1, Exp. 2) was designed to assess the behavior of tissue cells after treatment of the surfaces. Experiment 3 (Figure 1, Exp. 3) aimed to evaluate the colonization by tissue cells human gingival fibroblast (hGF) of successfully decontaminated implant surfaces evaluating their morphology, vitality, and cytocompatibility.

In the 2D peri-implant mucosa model (Figure 1), 10 discs were exposed to the multispecies bacteria, and biofilms were formed. Then, 5 were used in Exp. 1 and Exp. 5 in Exp. 3, whereas Exp. 2 used five discs without inoculating bacteria (15 discs in total). Subsequently, the proposed decontamination methods (CUR, XN, GS) and phosphate buffer saline (PBS, as negative control) and CHX (as positive control) were applied to one disc in each experiment. After 2 min of treatment and thorough washing hGF cells were seeded in Exp. 2 and Exp. 3. Then, all samples were assayed

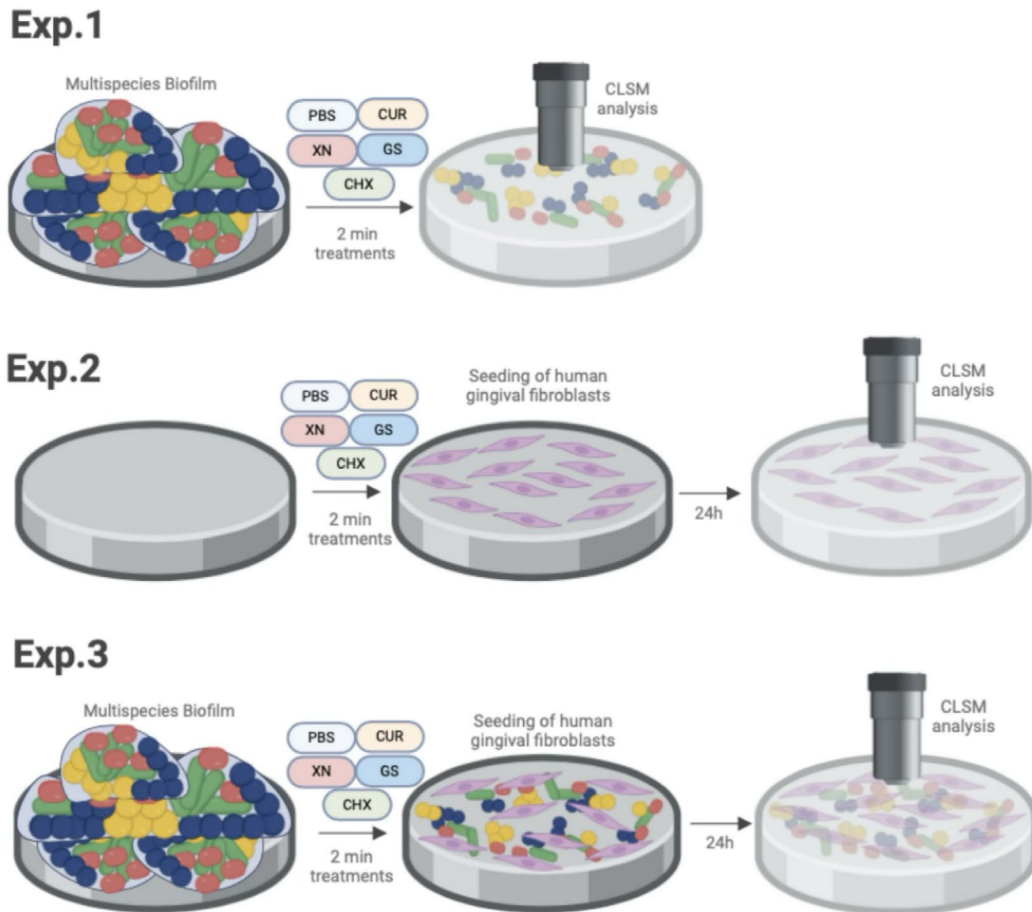


FIGURE 1 | Schematic illustration of the 2D model Experiment 1 (Exp. 1), Experiment 2 (Exp. 2), and Experiment 3 (Exp. 3). CHX, chlorhexidine; CLSM, confocal laser scanning microscopy; CUR, curcumin; GS, electrolytic treatment; PBS, phosphate buffer saline; XN, xanthohumol.

for bacterial and/or cell adhesion assessment by microscopical analysis. Each experiment was repeated five times, independently.

2.2 | Experiment Design Using the 3D Peri-Implant Mucosa Model

The peri-implant oral mucosa model assembly was based on the model developed in Hannover Medical School (Ingendoh-Tsakmakidis et al. 2019; Mikolai et al. 2020) with slight modifications.

In brief, hGF cells (passage 9 or 10) were added to a collagen hydrogel and poured into culture inserts (PIHA 03050, Merck Millipore or 3414, Corning B.V. Life Sciences). Titanium samples were pre-colonized with hGF cells (1×10^6 cells/mL). At day 5, titanium samples were integrated into the fibroblast-collagen gel. For this purpose, the models were punched with a 2.5 mm diameter biopsy punch and the titanium samples were placed in the resulting holes. After 3 days, 1.2×10^6 oral keratinocytes (OKF6/TERT-2, Passages 19–26) were seeded on the top of each fibroblast-collagen gel. At day 12, the models were raised to an air-liquid interface and cultivated for 13 days with a specific Airlift (AL) medium to obtain a multilayered peri-implant mucosa model (Figure 2A). These 3-D models were used in each replication (Figure 2, Exp. 4), one for each of the tested treatment groups.

For testing implant-decontamination procedures, co-cultures of the 3D mucosa with a multispecies biofilm were performed. First, the 3D model was washed with PBS prior to co-culture. Then, a mixture of four bacterial species taken from agar plates was smeared on each titanium insert (Figure 2B). Airlift was continued with AL-medium without antibiotics. A drop of BHI was placed on top of the biofilm-contaminated end of the insert (to keep it moist and nutrified) and was replaced every day. Then, one sample of each experiment was treated with one of four different decontamination protocols (CUR, XN, GS, CHX) and one more with PBS as a negative control (Figure 2C). After 2 min of treatment, analyses of all samples microscopically for bacterial and/or cell adhesion assessment took place (Figures 2D,E and S1). Exp. 4 was also repeated five times.

2.3 | Experimental Procedures

2.3.1 | Titanium Samples

Titanium discs (machine-cut from 12 mm diameter bars to 3 mm thickness) were utilized for testing in all 2D experimental setups (Exp. 1, Exp. 2, and Exp. 3). For the 3D experiment, titanium inserts (machine-cut from 3 mm diameter bars to 4.5 mm thickness) were used (Exp. 4). Titanium material fulfilled the requirements for grade 4 commercially pure titanium (standards ISO 5832-2 and ASTM f67). The surface was polished with an area

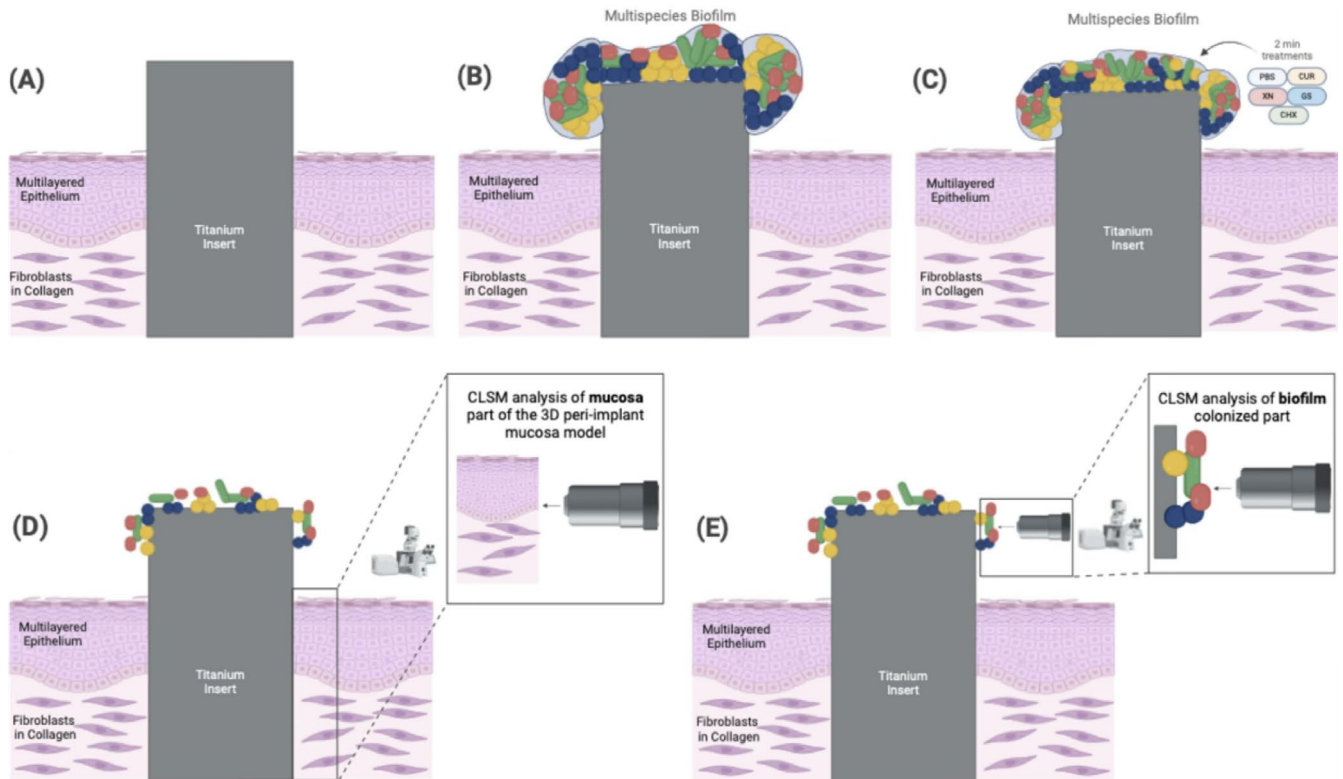


FIGURE 2 | Schematic illustration of Experiment 4 (Exp. 4): (A) 3D model; (B) co-culture of the 3D peri-implant mucosa model with the multispecies biofilm; (C) application of decontamination protocols on the titanium inserts of the 3D peri-implant mucosa biofilm model; confocal laser scanning microscopy (CLSM) analysis of the 3D models, including two different areas of analysis: (D) mucosa part and (E) biofilm colonized part. PBS, phosphate buffer saline; CUR, curcumin; XN, xanthohumol; GS, electrolytic treatment; CHX, chlorhexidine.

roughness (SA) value of 1.3 μm . All samples were autoclaved before their use.

2.3.2 | Bacterial Strains

Streptococcus oralis (ATCC 9811) was obtained from the American Type Culture Collection (Manassas, Virginia, USA). *Actinomyces naeslundii* (DSM 43013), *Veillonella dispar* (DSM 20735), and *Porphyromonas gingivalis* (DSM 20709) were obtained from the German Collection of Microorganisms and Cell Cultures (Braunschweig, Germany).

Bacteria were grown on blood agar plates (Blood Agar Oxoid No 2; Oxoid Limited, Wesel, Germany), supplemented with 5% (v/v) sterile horse blood (Oxoid Limited), 5.0 mg/L hemin (Sigma-ALDRICH Steinheim, Germany) and 1.0 mg/L menadione (Merck) in anaerobic conditions (10% H_2 , 10% CO_2 , and balance N_2) at 37°C for 24–72 h. They were then stored as glycerol stocks at -80°C and precultured in brain heart infusion medium (BHI; Oxoid Limited) supplemented with 10 $\mu\text{g}/\text{mL}$ vitamin K (Carl Roth GmbH & Co. KG, Karlsruhe, Germany).

2.3.3 | Cultivation of Multispecies Biofilm

A multispecies biofilm was grown on titanium surfaces as previously reported by Kommerein et al. (2017). Briefly, the four different bacterial pre-cultures were adjusted to an optical density

at 600 nm of 0.01 per bacterium. Then, they were mixed with equal volumes in BHI/vitamin K medium supplemented with 5 mg/L hemin.

The titanium discs for the 2D experiment were positioned in sterile 24-well plates (Greiner Bio-One International GmbH, Kremsmünster, Austria). Each well was inoculated with 1 mL of the bacterial suspension and incubated under anaerobic conditions (10% H_2 , 10% CO_2 , and N_2 in balance) at 37°C for 24 h. Regarding the 3D experiment, 1 mL of the four bacteria mixture was spread on blood agar plates and grown for 24 h. From these, a mixed colony was taken with a loop and smeared on the titanium insert.

2.3.4 | Titanium Decontamination

All treatments of samples were performed by one trained operator (A.A.-E). Decontamination protocols consisted on the application of the chemical product or the treatment with an electrolytic device, thus creating the following treatment groups in each experiment: PBS, as negative control; 5 mM CUR (Sigma-ALDRICH Steinheim, Germany); 100 μM XN (NATECO GmbH&Co, Wolnzach, Germany); electrolytic decontamination (GalvoSurge – GS) and CHX as positive control (Dynexidin Forte oromucosal solution 0.2%, Kreussler & Co. GmbH, Chemische Fabrik, Wiesbaden, Germany). CHX was applied as a ready-to-use mouth rinse. Concentrations of CUR and XN were selected according to their minimum inhibitory

concentrations (MIC) and minimum bactericidal concentrations (BIC) against biofilm-forming bacterial strains, as defined in a previous study (Alonso-Espanol et al. 2023). GS was used by placing the tip of the device directly in contact with the titanium sample.

Samples were rinsed twice with 2 mL of PBS before the treatments (10 s immersion per wash) and once after the treatments. Care was taken to ensure that titanium was equally and completely covered by the agents without mechanical detachment of the biofilm. All decontamination procedures lasted 2 min per treatment.

2.3.5 | Eukaryotic Cell Culture

Human gingival fibroblasts (121 0412, Provitro AG, Berlin, Germany) (passage 9) were cultured in Dulbecco's modified Eagle's medium (DMEM, FG0435, Biochrom AG), supplemented with 10% fetal bovine serum (FBS, P30-3309, PAN-Biotech GmbH, Aidenbach, Germany), 100 U/mL penicillin, and 100 µg/mL streptomycin (A2212; Biochrom AG, Berlin, Germany). The cells were incubated at 37°C in a 5% CO₂ humidified atmosphere.

The immortalized human oral keratinocyte cell line (OKF6/TERT-2; Dickson et al. 2000) was cultured in KerSFM medium (10725-018, Gibco, Fisher Scientific, Schwerte, Germany), supplemented with 0.3 mM CaCl₂, 0.2 mg/mL EGF, 25 µg/mL BPE, 100 U/mL penicillin, and 100 µg/mL streptomycin.

2.3.6 | CLSM Analysis

After the treatments, the multispecies biofilms and cells were washed once with PBS. They were then stained with the LIVE/DEAD BacLight Bacterial Vitality Kit (SYTO9 and propidium iodide dyes, Life Technologies, Carlsbad, CA, USA) and with Calcein-AM (Sigma-ALDRICH) according to the manufacturer's instructions. Stained biofilms/cells were then observed with a CLSM (Leica TCS SP8, Leica Microsystems, Mannheim, Germany). SYTO9 and Calcein-AM were excited using a 488 nm laser line and emission was detected at 500–550 nm. Propidium iodide was excited using a 552 nm laser line and emission was detected at 650–750 nm. In addition, surface reflection was detected at 485–490 nm. For each sample, at least five z-stack images were acquired with a z-step size of 5 µm for both X10 and X40 magnification. The ImageJ2 2.14.0/1.54f software package (Rasband 2012) was used to calculate the total surface coverage percentage and the percentage of LIVE/DEAD distribution. For this purpose, the integrity (SYTO9; green) or non-integrity (propidium iodide; red) of the cell membrane, and colocalized (SYTO9 + propidium iodide; green + red) areas of the resulting biofilms were quantified. As propidium iodide could enter the cells, colocalized areas were counted as dead and subtracted from the viable proportion.

Surface coverage analysis by ImageJ2 provided data on the overall coverage, including both bacteria and cells. To additionally obtain the percentage of titanium surface just covered

by eukaryotic cells, a neural network image analysis (Cellpose package—anatomical segmentation algorithm) was used as previously described by Stringer et al. (2021), Stringer et al. (2021). Example images of segmented cells are shown in Figure S2. With this neural network, it was possible to differentiate the surface just covered by hGF cells and subtract it from the whole amount of coverage by biofilm and cells.

2.4 | Statistical Analysis

Each individual experimental setup/decontamination combination resulted in $N=5$ technical replicates, analyzed in $N=5$ microscopic images. Thus, the total N accounts for 25 per experiment. Data analysis was done using SPSS (IBM SPSS Statistics 27.0, IBM Corporation, Armonk, NY, USA) and data presentation with GraphPad Prism software (9.2.0v, GraphPad Software, San Diego, California, USA). The Shapiro–Wilk goodness-of-fit test was used to assess for normality in the data distribution. Comparisons were tested applying one-way ANOVA tests with post hoc Bonferroni corrections for each of the experiments. Statistically significant differences were considered for p -values <0.05 . Data were expressed as means with standard deviations (SD).

3 | Results

3.1 | Antibacterial Effect of the Different Decontamination Procedures on Multispecies Biofilms in a 2D Model (Exp. 1)

The quantitative results from the decontamination procedures in Exp. 1 were depicted as total percentage of surface covered by bacteria and percentage of living bacteria, as shown in Table S1. The treatments with CUR, XN, GS, and CHX led to statistically significant reductions in the proportion of living bacteria, when compared with the PBS control group (Figure 3A). CUR and XN caused the highest shifts in the percentage of reduction of living bacteria, compared with PBS (82.70% and 82.10%, respectively), followed by GS and CHX (77.23% and 78.30%, respectively). In terms of percentage of surface covered, XN had the highest effect, demonstrating statistically significant differences between XN-PBS and XN-CHX after post hoc Bonferroni corrections (Figure 3B and Table S1). The antibacterial effect evaluated by CLSM analysis depicted a higher disruption of the biofilm biomass by CUR and XN (Figure 3D,E, respectively), while GS showed a “bubble-shaped effect”, depicting localized areas in the discs covered with a non-vital biofilm, together with adjacent areas of higher antimicrobial activity where biofilm biomass has been completely cleared (Figure 3F).

3.2 | Effect of the Different Decontamination Methods on Subsequent Tissue Cell Adhesion in a 2D Model (Exp. 2)

The results in percentage of surface covered by hGF cells after the exposure of the titanium discs to the four treatments, evaluated by quantitative CLSM is shown in Table S2. GS and CHX

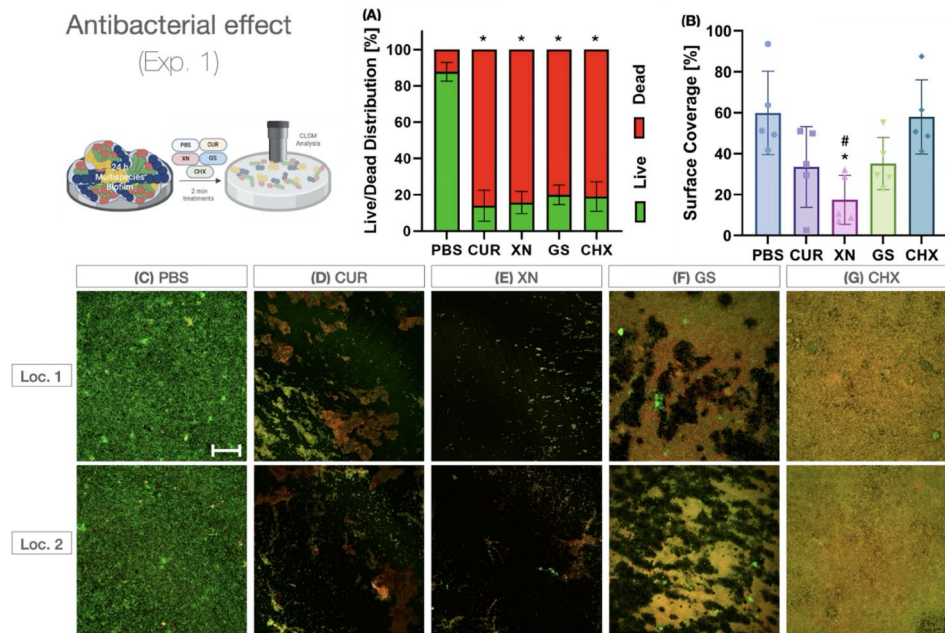


FIGURE 3 | Effectiveness of decontamination procedures on multispecies biofilms as 2D model analyzed by LIVE/DEAD and calcein staining (Experiment 1): (A) LIVE/DEAD distribution percentage: * $p < 0.05$ of all the experimental groups versus PBS control; (B) surface coverage percentage: * $p < 0.05$ to PBS as negative control; # $p < 0.05$ to CHX as positive control; (C–G) representative microscopic images of the different experimental groups. Locations (Loc.) 1 and 2 are from one sample. Viable bacteria are shown in green; dead bacteria are shown in orange/red. Microscope objective X40. Scale bar = 50 μm . CHX, chlorhexidine; CUR, curcumin; GS, electrolytic treatment; PBS, phosphate buffer saline; XN, xanthohumol.

showed a decreased cell adhesion, although without being statistically significant (Figure 4A,E,F and Table S2). XN and the negative control (PBS) stimulated surface coverage by cells (Figure 4B,D); in contrast, CUR still resulted in a trend towards reduced cellular adhesion (Figure 4C). Regarding cell morphology, compared to the PBS control, there were more rounded cells or cells without cytoplasm observed for CUR, GS, and CHX (Figure 4C,E,F, respectively).

3.3 | Effect of the Different Decontamination Methods on Cell Adhesion After Multispecies Biofilm Removal in a 2D Model (Exp. 3)

In the third 2D experiment, the results on the effect of the different decontamination methods on the multispecies biofilm were evaluated by measuring multispecies biofilm removal and subsequent cell adhesion, as shown in Table S3. These results confirmed previous observations from Exp. 1, with CUR, XN, GS, and CHX demonstrating a significant antimicrobial effect, with reductions in viable counts of 75.06%, 74.70%, 67.16%, and 77.68%, respectively, when compared with the PBS control group (Figure 5A).

In contrast to Exp. 1, where significant reductions in the percentage of surface coverage were only observed in the XN group, in Exp. 3, CUR and XN treatments led to statistically significant reductions in surface coverage, versus the positive control, CHX (Figure 5B). GS-treated samples showed also a decrease in biofilm, but to a lower extent and not being significantly different when compared with the other groups (Figure 5B,G). CHX

showed a similar surface coverage to the negative control (PBS), indicating that biofilm biomass was not disrupted by this treatment (Figure 5B,H).

The analysis of the microscopic images depicted that in the PBS group, an intact and completely viable biofilm prevented hGF cells from colonizing the titanium surfaces, (Figure 5D). CUR and XN enabled a certain amount of cell attachment (Figure 5E,F, respectively). CUR treatment depicted changes in the cell morphology and loss of the cytoplasm, indicating a higher degree of cytotoxicity or less cytocompatibility, compared with XN (Figure 5E). In the GS group, the number of viable cells after 24h of cultivation seemed reduced, with the presence of the cells adhering to the titanium discs in areas where the biofilm biomass had been removed (Figure 5G). The “bubble-shaped effect”, described in Exp. 1, enabled the attachment of hGF cells; however, in adjacent areas with severe remains of nonvital biofilms, there was a clear negative impact of GS-treated surfaces on cell attachment (see Exp. 2 and Figure 5G). Almost no fibroblasts were able to adhere after CHX treatment (Figure 5H) and the few cells identified demonstrated signs of loss vitality, due to morphology alterations and loss of cytoplasm.

To quantify the attachment and subsequent proportion of titanium surface covered only by fibroblasts, in images with mixed coverage of bacterial biofilm and tissue cells after decontamination treatments, neural network analysis was applied (Figure S2). There was a clear trend towards less number of cells on the surface of the titanium after PBS and CHX treatments, although no statistically significant differences

Effect on subsequent tissue cell adhesion (Exp. 2)

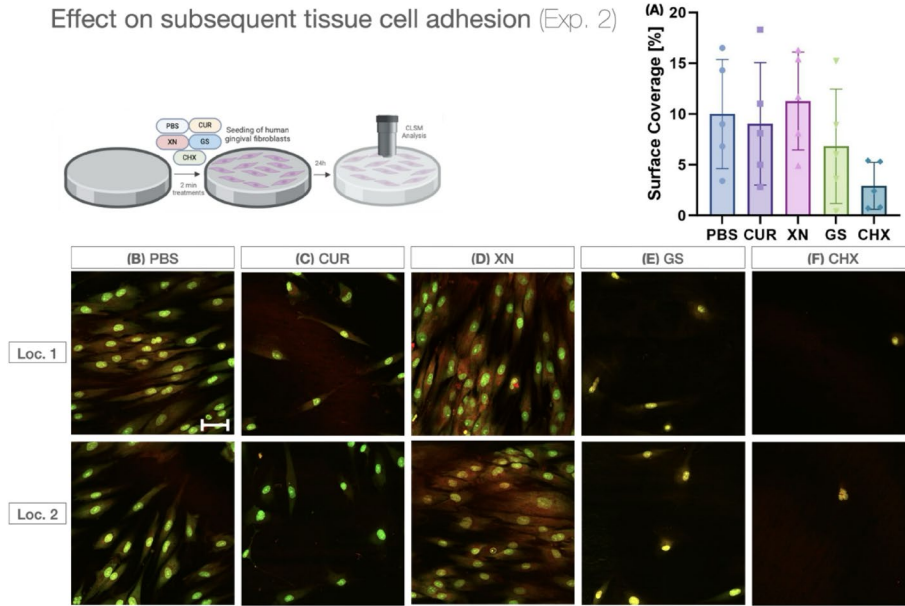


FIGURE 4 | Effect of decontamination procedures on subsequent tissue cell adhesion in a 2D model analyzed by LIVE/EAD and calcein staining (Experiment 2): (A) surface coverage percentage, no statistically significant differences were detected; (B–F) representative microscopic images of the different experimental groups. Location (Loc.) 1 and 2 are from one sample. Microscope objective X40. Scale bar = 50 μm. PBS, phosphate buffer saline; CUR, curcumin; XN, xanthohumol; GS, electrolytic treatment; CHX, chlorhexidine.

Effect on cell adhesion after biofilm removal (Exp. 3)

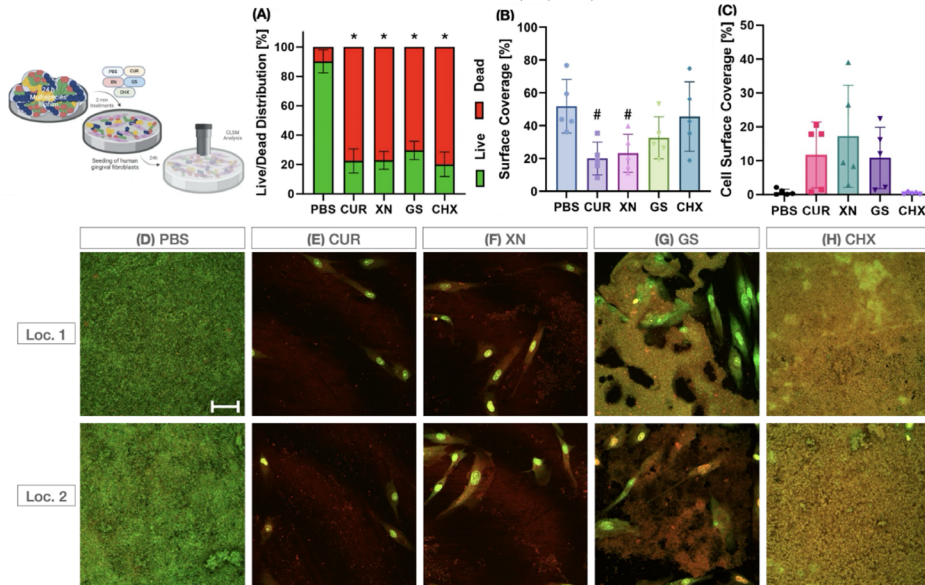


FIGURE 5 | Effect of decontamination methods on cell adhesion after multispecies biofilm removal in a 2D model (Experiment 3): (A) LIVE/DEAD distribution percentage: $*p < 0.05$ of all the experimental groups versus PBS control; (B) surface coverage percentage: $\#p < 0.05$ to CHX as a positive control; (C) cell surface coverage percentage: No statistically significant differences were observed; (D–H) representative microscopic images of the different experimental groups. Locations (Loc.) 1 and 2 are from one sample. Viable bacteria and cells are shown in green; dead bacteria and cells are shown in orange/red. Microscope objective X40. Scale bar = 50 μm. CHX, chlorhexidine; CUR, curcumin; GS, electrolytic treatment; PBS, phosphate buffer saline; XN, xanthohumol.

between the treatment protocols were found. As depicted in Figure 5C, higher percentages of hGF cell surface coverage were demonstrated in CUR, XN, and GS. Overall, when less bacteria were present on the surface, there were higher

chances for hGF cells to colonize. Also, the presence of a completely viable biofilm prevented hGF colonization, while the presence of higher proportions of dead bacteria allowed some tissue cell attachment.

3.4 | Effect of the Different Decontamination Methods on Tissue Cells and Biofilm in the 3D Co-Culture Model (Exp. 4)

3.4.1 | Effect on the Peri-Implant Mucosa Area of the 3D Model

The CLSM results, expressed as percentages of viable hGF cells in the 3D mucosa model, the integrity of the mucosa, as well as the percentages of surface covered by tissue cells, after the exposure to the different decontamination groups on the peri-implant mucosa, are illustrated in Figure 6 and Table S4.

The impact on cell vitality of CUR and XN was minimal, with reductions of 5.18% and 4.29%, respectively (Figure 6A). However, when compared to the negative control (PBS), GS and CHX showed significant reductions of 84.86% and 87.67% vital cells, respectively (Figure 6A). After post hoc Bonferroni corrections, statistically significant differences were also found between GS versus CUR, XN, and PBS (Figure 6A). The percentage of surface covered by the cells showed the same tendency among the groups, without any statistically significant difference (Figure 6B).

Regarding tissue integrity, as observed in the microscopic images, the peri-implant mucosa without treatment (PBS control) showed tissue integrity, with maintenance of the different tissue layers (Figure 6C) depicting on top an intact and densely packed epithelium layer, with a mix of green and yellow appearing cells (keratinocytes) and underneath an area with dispersed green cells (hGF cells) within the hydrogel. CUR and XN groups also depicted the different layers of keratinocytes and hGF cells (Figure 6D,E, respectively). However, in the 3D peri-implant mucosa after GS and CHX treatments, as shown in Figure 6F,G, there was a disruption of the structural layers. Specifically, in the GS group, there was partial removal of the mucosa from the implant surface, indicating the loss of implant–mucosa binding (as observed in Figure S1D).

3.4.2 | Effect on the Biofilm Formed on Titanium Surfaces Within the 3D Model

Figure 7 and Table S5 depict the results of different decontamination protocols on the biofilms formed on the titanium area of the insert evaluated with quantitative CLSM.

In terms of bacterial viability, the results in the 3D co-culture setting confirm the observations reported in Exp. 1, with a

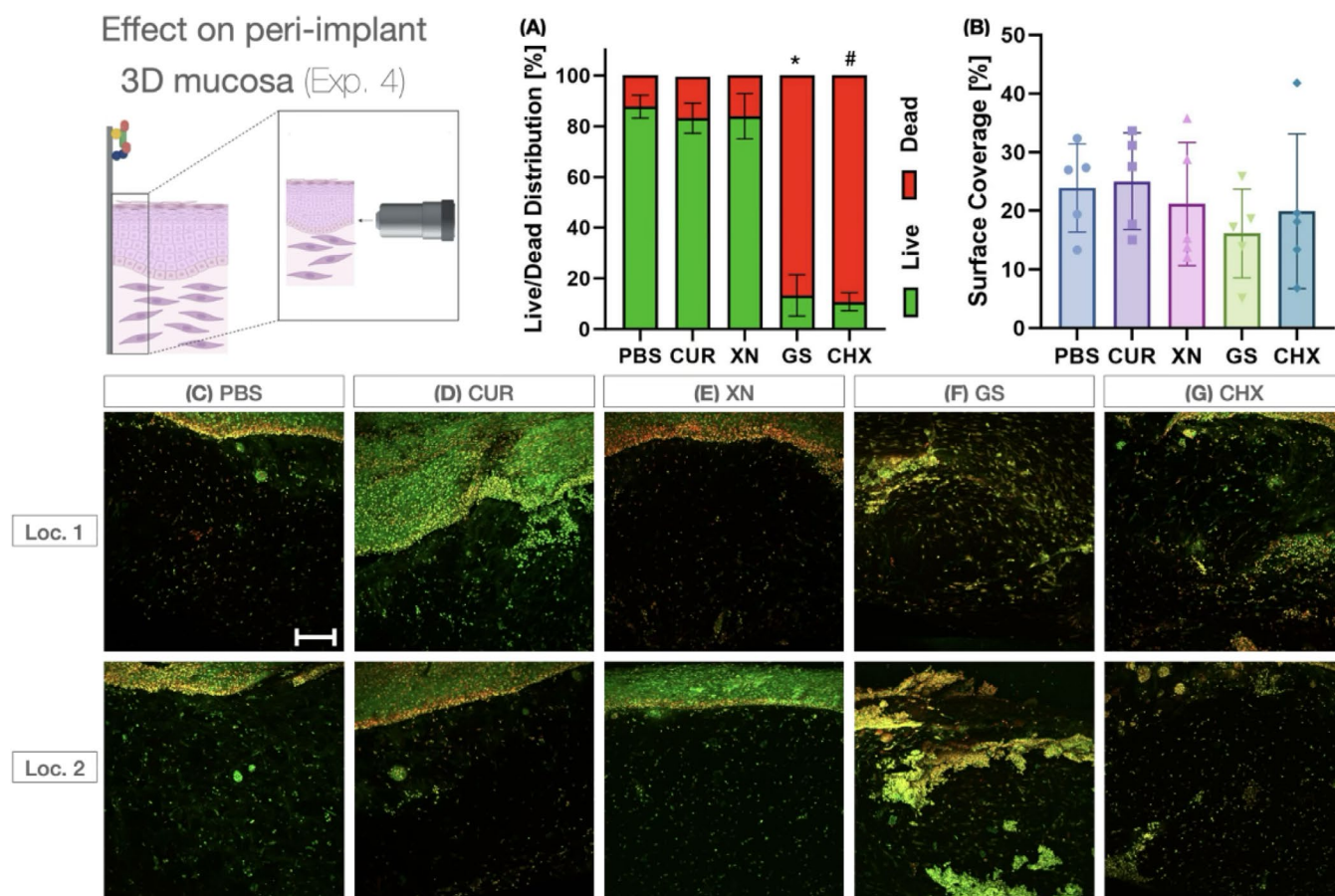


FIGURE 6 | Effect of decontamination methods on the peri-implant mucosa area of the 3D model: (A) LIVE/DEAD distribution percentage: * $p < 0.05$ versus CUR, XN, and PBS; # $p < 0.05$ versus CUR, XN, and PBS; (B) surface coverage percentage: No statistically significant differences were observed; (C–G) representative microscopic images of the different experimental groups. Locations (Loc.) 1 and 2 are from one sample. Viable bacteria and cells are shown in green; dead bacteria and cells are shown in orange/red. Microscope objective X10. Scale bar = 200 μm . CHX, chlorhexidine; CUR, curcumin; GS, electrolytic treatment; PBS, phosphate buffer saline; XN, xanthohumol.

Effect on titanium colonisation by multispecies biofilm on 3D model (Exp. 4)

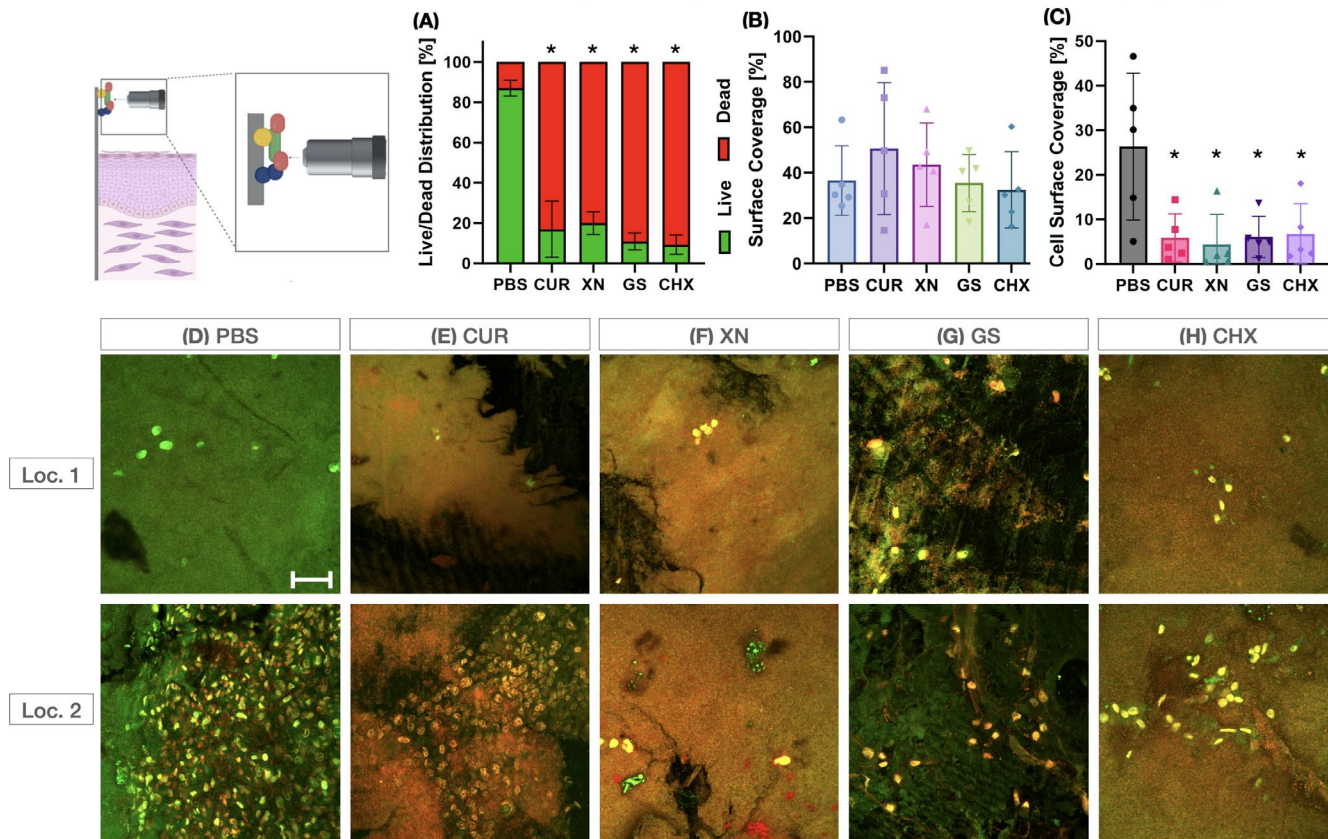


FIGURE 7 | Effect of decontamination methods on the titanium colonization by multispecies biofilm of the 3D model: (A) LIVE/DEAD distribution percentage: $*p < 0.05$ of all the experimental groups versus PBS control; (B) surface coverage percentage: No statistically significant differences were observed; (C) cell surface coverage percentage: $*p < 0.05$ of all the experimental groups versus PBS control; (D–H) representative microscopic images of the different experimental groups. Locations (Loc.) 1 and 2 are from one sample. Viable bacteria and cells are shown in green; dead bacteria and cells are shown in orange/red. Microscope objective X40. Scale bar = 50 μm. CHX, chlorhexidine; CUR, curcumin; GS, electrolytic treatment; PBS, phosphate buffer saline; XN, xanthohumol.

significant decrease in viability after the four decontamination protocols (Figure 7A). Similarly, the evaluation of the percentage of surface coverage resulted in comparable results (Figure 7B). The negative control group depicted mainly bacteria but also some hGFs cells directly on the titanium (Figure 7E), while in the treated samples, the biomass consisted of a combination of mainly dead bacteria and hGFs cells (Figure 7E–H). GS depicted again the referred “bubble-shaped effect”, combining areas with intense antimicrobial activity and areas with remaining biomass subsequently covered with hGFs cells (Figure 7G). With the use of neural networks, it was confirmed that the negative control groups allow the attachment of significantly higher number of cells than the rest of treatments (Figure 7C).

4 | Discussion

This in vitro investigation has evaluated the antibacterial effects and the impact on cytocompatibility of three implant surface decontamination methods (CUR, XN, and GS) on multispecies biofilms developed in both 2D and 3D peri-implant mucosa models, when compared to a negative (PBS) and a positive (CHX) control method. The antibacterial effect assessed in Experiment 1 showed a significant antimicrobial effect of the three treatment

groups and the positive control, when compared to the negative control group, mainly in terms of reducing the proportion of living bacteria, although XN, followed by CUR had the highest effect in terms of the impact on the surface covered with biofilm. The alteration of the recolonization of tissue cells reported as the percentage of surface covered by hGFs cells after exposing the titanium discs to the different treatments was evaluated in Experiment 2. CHX demonstrated a significant alteration of viability with a significant decrease in cell adhesion. Similarly, GS showed a clear detrimental effect on tissue cell vitality, but in distinct areas within the discs. In contrast, CUR, XN, and the negative control group (PBS) did not show alterations of tissue cell viability, with assessment of the discs covered with viable tissue cells. Experiment 3 evaluated the extent to which successful decontamination of implant materials can lead to improved colonization by tissue cells. The results confirmed that the four interventions tested had a significant antimicrobial effect, when compared with the PBS control group. This differential antimicrobial effect influenced the cytocompatibility of the different treatments, since in the PBS group, an intact and completely viable biofilm prevented hGF cells from colonizing the titanium surfaces. Similarly, no viable fibroblasts were able to adhere to the titanium after CHX treatment (Figure 5H) due to its effect on the alteration of cytocompatibility. CUR and XN demonstrated a

higher degree of cytocompatibility depicting attached cells with positive signs of vitality, while the GS group showed a “bubble-shaped effect”, with clear alteration of the viability of tissue cells in areas with a high antimicrobial effect, with adjacent areas showing signs of cytocompatibility. When using the 3D co-culture model, in the control group without treatment, the background showed attachment of live fibroblasts. In contrast, when the tested treatments were applied, the adherence of viable hGFs cells was significantly altered by the presence of a bio-mass, mainly composed of dead bacteria. However, while in the CUR and XN groups, there was a minimal impact on the mucosa structure and vitality, in the GS and CHX groups, there was a clear impact in the mucosa integrity, what evidenced their effect on the alteration of the cytocompatibility, previously described in the 2D model. These results confirmed the hypothesis.

The use of LIVE/DEAD staining does not allow for an accurate evaluation of eukaryotic cells, since these cells only intercalate with double-stranded deoxyribonucleic acid, and hence they do not stain sufficiently the whole cell body. The addition of calcein staining, was, therefore, applied to better discriminate the cellular body and the nucleus, as well as discriminate the impact of the treatments on cell morphology and integrity of the cell membranes.

These results clearly show that the impact of the different decontamination methods on tissue cells was directly influenced by their respective cytotoxic effect or indirectly through the effect of their relative antimicrobial effect on the titanium surfaces and subsequent cell colonization patterns. These effects demonstrated in the 2D peri-implant model were further corroborated in a modified 3D model (Ingendoh-Tsakmakidis et al. 2019; Mikolai et al. 2020), and the antimicrobial and cytotoxic effects of the tested interventions can be investigated simultaneously.

Previous in vitro studies have also reported the anti-microbial effect of different implant surface decontamination protocols using either physical or microbiological evaluation methods, such as removal of permanent ink coated over the implant surface (Luengo et al. 2022), or assessing their effect on mono (Batalha et al. 2021; Ichioka et al. 2021), or multispecies in vitro biofilm models (Cordeiro et al. 2021; Eick et al. 2017; Leung et al. 2022). However, none of these studies evaluated the combined effect of these interventions on contaminated titanium discs using biofilms and living cells in co-culture using well-designed in vitro mucosa model's relevance for the treatment of peri-implant diseases in humans. To overcome this limitation, we used in the present study a modification of the preexistent 2D model (Kommerein et al. 2017), combining hGF cells in co-culture with a treated multispecies biofilm. Furthermore, we used a well-established multispecies biofilm model consisting of *S. oralis*, *A. naslundii*, *V. dispar*, and *P. gingivalis* (Kommerein et al. 2017).

The reported in vitro antimicrobial and antibiofilm effects of the two natural extracts used (CUR and XN) have been previously reported, using mono-species biofilm models of *Aggregatibacter actinomycetemcomitans* and *P. gingivalis* (Maleki Dizaj et al. 2022), as well as multi-species biofilms (Alonso-Espanol et al. 2023), in which a clear bactericidal effect of CUR and XN on the six bacteria tested forming a mature biofilm was

observed. This effect was similar compared to CHX, and even slightly higher for some of the bacterial species used in this in vitro biofilm model. Their mechanism of action has been attributed to its inhibiting effect on dipeptidyl peptidases, which interferes with the bacteria nucleic acid synthesis and central metabolic pathways (Murai et al. 2024).

In vitro studies with mono-species, multispecies, and natural biofilms have also been used to evaluate the efficiency of different electrochemical implant-decontamination methods (Al-Hashedi et al. 2016; Sahrman et al. 2014). These studies have shown significant bacterial and biofilm reductions. However, these investigations have applied different electrochemical parameters in terms of the current (continuous versus alternate), amperage (from 3 to 600 mA) and the electrolyte used. Our research group has recently reported a clear bactericidal effect on a multispecies subgingival in vitro biofilm model, when using an electrochemical construct using currents of 12.9 mA (Virto et al. 2023). In this investigation, however, we used a commercially available implant-decontamination device, also based on the same electrolytic concept (GS) but using high electrical currents (600 mA). GS has been evaluated both in preclinical (Assuncao et al. 2023) as well as in clinical studies demonstrating its efficacy to detach biofilms adhered to implant surfaces (Schlee et al. 2019, 2021). Its mechanism of action is based on the hydrolysis of the surrounding liquid by the applied electric energy, what releases highly reactive substances such as I_2 , H_2O_2 , and hydroxyl radicals with proven antimicrobial activity (Ehrensberger et al. 2015; Schneider et al. 2018; Wang et al. 2013). Also, the resulting changes in pH and temperature, as well as the gas formed in the local environment, may also explain its “bubble-shaped effect” what leads to physical detachment of the biofilm in localized surface areas (del Pozo et al. 2009; Mohn et al. 2011). However, there is scarce knowledge on the likely direct and indirect impact of this applied electrochemical effect on the adjacent peri-implant tissues.

Similarly, the use of CHX has shown a significant antimicrobial effect in multiple clinical settings (Loesche 1979; Sekino et al. 2003), and hence, it is usually used as positive control in both in vitro and in vivo studies. However, in this investigation, the CHX treatment did not elicit a significant decrease in the implant surface biofilm coverage. This effect can be explained by the lack of effect of CHX on the biofilm matrix, since its main antibacterial mechanism is based in the ability of this molecule to bind reversibly to oral tissues (Bonesvoll, Lokken, and Rolla 1974; Bonesvoll et al. 1974) and slowly release a molecule that interferes with bacterial vitality. Hence, despite a significant reduction in the biofilm vitality, the biofilm biomass was not reduced, as it has been demonstrated in previous studies (Martinez-Hernandez, Reda, and Hannig 2020). Furthermore, different studies have reported the cytotoxicity of CHX on different cell types such as fibroblasts and osteoblasts using simplified cell culture conditions (Brunello et al. 2021; Giannelli et al. 2008; Kotsakis et al. 2016; Lee et al. 2010; Monje et al. 2022; Stein et al. 2023). This combined effect of cytotoxicity and the inability to remove the biofilm biomass by CHX resulted in a synergistic effect on cell behavior since it prevented their attachment and affected the integrity of the 3D peri-implant mucosal construct (Kozlovsky et al. 2006; Ryu et al. 2015).

In contrast, the two natural extracts used, CUR and XN, demonstrated a higher cytocompatibility, favoring fibroblast cell adhesion and preservation of their integrity and vitality. This effect can be explained by their mechanism of action, mainly through inhibiting *quorum sensing* and cell wall destabilization (Adamczak, Ozarowski, and Karpinski 2020; Hu, Huang, and Chen 2013; Leoni and Landini 2014; Sakai et al. 2012). Since eukaryotic cells lack these targets, CUR and XN have a higher cytocompatibility compared with CHX. When comparing the differential effect on the cells by CUR and XN, XN demonstrated a better cytocompatibility, since fibroblasts depicted morphological signs of cell damage after CUR treatment. These results are to some extent in contradiction with a previous study in which CUR nanoparticles and CUR with and without photoactivation did not alter the cytocompatibility of periodontal ligament fibroblast cells, but at the same time showed antimicrobial and antibiofilm-like properties (Tonon et al. 2022). In this study, up to 500 µg/mL CUR were used and these higher concentrations could explain these differential effects on cytocompatibility. With GS treatment, the biofilm was only partially removed and the cells mainly settled in these freed areas. The treatment also led to changes in the implant material, which often resulted in a rounder cell morphology. Although there is not much information found in the literature that gives an explanation to this, it might be related to changing surface groups, changing crystal structure, distribution of the titanium grains, or charging of surface (Ciarolla et al. 2022). In all cases, it was very clear that the antibacterial capacity of the individual treatments increased obviously when fibroblasts subsequently seeded and successfully attached to the surfaces. Similar observations of an improved cytocompatibility and simultaneously increased antibacterial effects in co-culture conditions have been described before (Doll-Nikutta et al. 2024). This highlights the relevance of co-culture models when the effects on peri-implant infections are the subject of investigations in vitro.

The experiments with the modified 3D model allowed us to study the direct effects of the different decontamination procedures in a peri-implant co-culture setting that includes a multi-species biofilm as well as a structured mucosa, which is clearly a step closer to the anticipated clinical situation (Ingendoh-Tsakmakidis et al. 2019; Mikolai et al. 2020). This model reiterated the results reported with the 2D model demonstrating a net cytotoxic effect after CHX application. Also, the GS treatment showed clear antibacterial and cytotoxic effects in this 3-D model with disruption of the tissue layers and even detachment of the entire tissue from the titanium surfaces. In contrast, CUR and XN preserved the integrity of the mucosa structural layers even in a direct application. However, in this 3D co-culture setting, both substances also demonstrated less antimicrobial effect than in the 2D experiments, especially regarding the ability to remove the biofilm. This differential effect can be attributed to the interference of the living cells with the antibiofilm effect of the natural extracts.

The strength of this in vitro investigation resides in the use of a complex construct to study the concomitant antimicrobial and cytotoxic effect of different implant surface decontamination methods, demonstrating that a chemical (CHX) or electrochemical (GS) treatment with proven antimicrobial effects

showed direct and indirect deleterious effects on living tissues. Conversely, the use of phytotherapeutics (CUR and XN) demonstrated a similar antimicrobial and antibiofilm effect with a significantly higher cytocompatibility. However, despite using 3-D peri-implant mucosa models, the in vitro nature of this investigation does not allow a direct translation of these results to the clinical practice. Further in vivo studies are needed to evaluate the concomitant antimicrobial and tissular effects of commonly used implant surface decontamination protocols. Besides, using GS on a 2D sample (discs or inserts) bears the risk to miss the effect that would occur over real dental implants, where the surface is not homogeneous, and hence, the density of the current would change from exposed areas like thread tips to less active areas like the valleys between the threads.

5 | Conclusions

Within the limitations of the present study, it can be concluded that all tested implant surface decontamination treatments showed statistically significant differences compared to the negative control in terms of antimicrobial activity. Phytotherapeutics, CUR and XN, were the most cytocompatible substances and showed the largest antimicrobial effect. GS displayed antibiofilm activity with a localized “*bubble-shaped effect*” and impaired hGFs cell morphology and integrity, compromising tissue cell cytocompatibility. CHX showed antimicrobial capacity, without reducing biofilm biomass and demonstrating altered cytocompatibility. As these effects have not only been observed in 2D but also in a 3D in vitro model, they are even more promising for future clinical studies.

Author Contributions

Andrea Alonso-Español: conceptualization, investigation, writing – original draft, writing – review and editing, visualization, validation, methodology, software, formal analysis, data curation. **Enrique Bravo:** conceptualization, writing – review and editing, supervision. **Ana Carrillo de Albornoz:** conceptualization, visualization, methodology, writing – review and editing, supervision. **María Martínez:** formal analysis, writing – review and editing, data curation. **Katharina Doll-Nikutta:** conceptualization, methodology, data curation, software, formal analysis, validation, supervision, investigation. **Andreas Winkel:** conceptualization, investigation, writing – review and editing, validation, methodology, visualization, project administration, supervision. **Meike Stiesch:** writing – review and editing, supervision, validation. **David Herrera:** writing – review and editing, supervision, validation. **Bettina Alonso:** writing – review and editing, supervision. **Mariano Sanz:** conceptualization, investigation, funding acquisition, writing – review and editing, validation, project administration, supervision, resources.

Acknowledgments

The authors thank Diana Strauch for her indispensable support and Nicolas Debener for the invaluable help with the Cellpose package. The authors also acknowledge the technical support of A.M. Vicente, at the ICTS National Centre of Electron Microscopy (University Complutense, Madrid, Spain). They also thank J. Arroyo and C. Nombela (R.I.P.), at the Faculty of Pharmacy (University Complutense, Madrid, Spain), for the lending of xanthohumol. The authors also express their gratitude for the funding provided by SEPA Foundation (*Beca de Investigación Sepa 2023. Estudios diseñados en el marco de la investigación básica, preclínica y clínica—Aula de Investigación SEPA 2023*).

Conflicts of Interest

The authors declare no conflicts of interest.

Data Availability Statement

The data that support the findings of this study are available from the corresponding author upon reasonable request.

References

- Adamczak, A., M. Ozarowski, and T. M. Karpinski. 2020. "Curcumin, a Natural Antimicrobial Agent With Strain-Specific Activity." *Pharmaceuticals (Basel)* 13, no. 7: 153. <https://doi.org/10.3390/ph13070153>.
- Al-Hashedi, A. A., M. Laurenti, M. N. Abdallah, R. F. Albuquerque Jr., and F. Tamimi. 2016. "Electrochemical Treatment of Contaminated Titanium Surfaces In Vitro: An Approach for Implant Surface Decontamination." *ACS Biomaterials Science & Engineering* 2, no. 9: 1504–1518. <https://doi.org/10.1021/acsbomaterials.6b00265>.
- Alonso-Espanol, A., E. Bravo, H. Ribeiro-Vidal, et al. 2023. "The Antimicrobial Activity of Curcumin and Xanthohumol on Bacterial Biofilms Developed Over Dental Implant Surfaces." *International Journal of Molecular Sciences* 24, no. 3: 335. <https://doi.org/10.3390/ijms24032335>.
- Assuncao, M. A., J. Botelho, V. Machado, et al. 2023. "Dental Implant Surface Decontamination and Surface Change of an Electrolytic Method Versus Mechanical Approaches: A Pilot In Vitro Study." *Journal of Clinical Medicine* 12, no. 4: 1703. <https://doi.org/10.3390/jcm12041703>.
- Batalha, V. C., R. A. Bueno, E. Fronchetti Junior, et al. 2021. "Dental Implants Surface In Vitro Decontamination Protocols." *European Journal of Dentistry* 15, no. 3: 407–411. <https://doi.org/10.1055/s-0040-1721550>.
- Berglundh, T., S. Jepsen, B. Stadlinger, and H. Terheyden. 2019. "Peri-Implantitis and Its Prevention." *Clinical Oral Implants Research* 30, no. 2: 150–155. <https://doi.org/10.1111/clr.13401>.
- Bonesvoll, P., P. Lokken, and G. Rolla. 1974. "Influence of Concentration, Time, Temperature and pH on the Retention of Chlorhexidine in the Human Oral Cavity After Mouth Rinses." *Archives of Oral Biology* 19, no. 11: 1025–1029. [https://doi.org/10.1016/0003-9969\(74\)90089-2](https://doi.org/10.1016/0003-9969(74)90089-2).
- Bonesvoll, P., P. Lokken, G. Rolla, and P. N. Paus. 1974. "Retention of Chlorhexidine in the Human Oral Cavity After Mouth Rinses." *Archives of Oral Biology* 19, no. 3: 209–212. [https://doi.org/10.1016/0003-9969\(74\)90263-5](https://doi.org/10.1016/0003-9969(74)90263-5).
- Bosshardt, D. D., U. R. Brodbeck, F. Rathe, et al. 2022. "Evidence of Re-Osseointegration After Electrolytic Cleaning and Regenerative Therapy of Peri-Implantitis in Humans: A Case Report With Four Implants." *Clinical Oral Investigations* 26, no. 4: 3735–3746. <https://doi.org/10.1007/s00784-021-04345-1>.
- Brunello, G., K. Becker, L. Scotti, D. Drescher, J. Becker, and G. John. 2021. "The Effects of Three Chlorhexidine-Based Mouthwashes on Human Osteoblast-Like SaOS-2 Cells. An In Vitro Study." *International Journal of Molecular Sciences* 22, no. 18: 986. <https://doi.org/10.3390/ijms22189986>.
- Carrillo de Albornoz, A., E. Montero, A. Alonso-Espanol, M. Sanz, and I. Sanz-Sanchez. 2024. "Treatment of Peri-Implantitis With a Flapless Surgical Access Combined With Implant Surface Decontamination and Adjunctive Systemic Antibiotics: A Retrospective Case Series Study." *Journal of Clinical Periodontology* 51: 968–980. <https://doi.org/10.1111/jcpe.13993>.
- Charalampakis, G., and G. N. Belibasakis. 2015. "Microbiome of Peri-Implant Infections: Lessons From Conventional, Molecular and Metagenomic Analyses." *Virulence* 6, no. 3: 183–187. <https://doi.org/10.4161/21505594.2014.980661>.
- Ciarolla, A. A., N. Lapin, D. Williams, R. Chopra, and D. E. Greenberg. 2022. "Physical Approaches to Prevent and Treat Bacterial Biofilm." *Antibiotics* 12, no. 1: 54. <https://doi.org/10.3390/antibiotics12010054>.
- Cordeiro, J. M., J. M. Pires, J. G. S. Souza, et al. 2021. "Optimizing Citric Acid Protocol to Control Implant-Related Infections: An In Vitro and In Situ Study." *Journal of Periodontal Research* 56, no. 3: 558–568. <https://doi.org/10.1111/jre.12855>.
- Cosgarea, R., A. Rocuzzo, K. Jepsen, A. Sculean, S. Jepsen, and G. E. Salvi. 2023. "Efficacy of Mechanical/Physical Approaches for Implant Surface Decontamination in Non-Surgical Submarginal Instrumentation of Peri-Implantitis. A Systematic Review." *Journal of Clinical Periodontology* 50, no. Suppl 26: 188–211. <https://doi.org/10.1111/jcpe.13762>.
- de Tapia, B., C. Valles, T. Ribeiro-Amaral, et al. 2019. "The Adjunctive Effect of a Titanium Brush in Implant Surface Decontamination at Peri-Implantitis Surgical Regenerative Interventions: A Randomized Controlled Clinical Trial." *Journal of Clinical Periodontology* 46, no. 5: 586–596. <https://doi.org/10.1111/jcpe.13095>.
- del Pozo, J. L., M. S. Rouse, J. N. Mandrekar, J. M. Steckelberg, and R. Patel. 2009. "The Electricidal Effect: Reduction of Staphylococcus and Pseudomonas Biofilms by Prolonged Exposure to Low-Intensity Electrical Current." *Antimicrobial Agents and Chemotherapy* 53, no. 1: 41–45. <https://doi.org/10.1128/AAC.00680-08>.
- Dickson, M. A., W. C. Hahn, Y. Ino, et al. 2000. "Human Keratinocytes that Express hTERT and also Bypass a p16(INK4a)-Enforced Mechanism that Limits Life Span Become Immortal Yet Retain Normal Growth and Differentiation Characteristics." *Molecular and Cellular Biology* 20, no. 4: 1436–1447. <https://doi.org/10.1128/MCB.20.4.1436-1447.2000>.
- Doll-Nikutta, K., N. Heine, M. Kheirmand-Parizi, et al. 2024. "Bacteria-Epithelial Cell Interaction Influences Cytotoxicity and Antibacterial Effect of Silver-Gold Alloy Nanoparticles on a Species-Specific Level." *ChemistryNanoMat* 10, no. 2: e202300400. <https://doi.org/10.1002/cnma.202300400>.
- Domisch, H., D. Hoedke, C. Valles, J. Vilarrasa, S. Jepsen, and A. Pascual La Rocca. 2023. "Efficacy of Professionally Administered Chemical Agents as an Adjunctive Treatment to Sub-Marginal Instrumentation During the Therapy of Peri-Implant Mucositis." *Journal of Clinical Periodontology* 50, no. Suppl 26: 146–160. <https://doi.org/10.1111/jcpe.13747>.
- Ehrensberger, M. T., M. E. Tobias, S. R. Nodzo, et al. 2015. "Cathodic Voltage-Controlled Electrical Stimulation of Titanium Implants as Treatment for Methicillin-Resistant *Staphylococcus aureus* Periprosthetic Infections." *Biomaterials* 41: 97–105. <https://doi.org/10.1016/j.biomaterials.2014.11.013>.
- Eick, S., I. Meier, F. Spoerle, et al. 2017. "In Vitro-Activity of er:YAG Laser in Comparison With Other Treatment Modalities on Biofilm Ablation From Implant and Tooth Surfaces." *PLoS One* 12, no. 1: e0171086. <https://doi.org/10.1371/journal.pone.0171086>.
- Gennai, S., J. Bollain, N. Ambrosio, C. Marruganti, F. Graziani, and E. Figuero. 2023. "Efficacy of Adjunctive Measures in Peri-Implant Mucositis. A Systematic Review and Meta-Analysis." *Journal of Clinical Periodontology* 50, no. Suppl 26: 161–187. <https://doi.org/10.1111/jcpe.13791>.
- Giannelli, M., F. Chellini, M. Margheri, P. Tonelli, and A. Tani. 2008. "Effect of Chlorhexidine Digluconate on Different Cell Types: A Molecular and Ultrastructural Investigation." *Toxicology In Vitro* 22, no. 2: 308–317. <https://doi.org/10.1016/j.tiv.2007.09.012>.
- Hakki, S. S., G. Tatar, N. Dundar, and B. Demiralp. 2017. "The Effect of Different Cleaning Methods on the Surface and Temperature of Failed Titanium Implants: An In Vitro Study." *Lasers in Medical Science* 32, no. 3: 563–571. <https://doi.org/10.1007/s10103-017-2149-2>.
- Herrera, D., T. Berglundh, F. Schwarz, et al. 2023. "Prevention and Treatment of Peri-Implant Diseases-The EFP S3 Level Clinical Practice

- Guideline." *Journal of Clinical Periodontology* 50, no. Suppl 26: 4–76. <https://doi.org/10.1111/jcpe.13823>.
- Hu, P., P. Huang, and M. W. Chen. 2013. "Curcumin Reduces *Streptococcus mutans* Biofilm Formation by Inhibiting Sortase A Activity." *Archives of Oral Biology* 58, no. 10: 1343–1348. <https://doi.org/10.1016/j.archoralbio.2013.05.004>.
- Ichioka, Y., J. Derks, G. Dahlen, T. Berglundh, and L. Larsson. 2021. "In Vitro Evaluation of Chemical Decontamination of Titanium Discs." *Scientific Reports* 11, no. 1: 22753. <https://doi.org/10.1038/s41598-021-02220-3>.
- Ingendoh-Tsakmakidis, A., C. Mikolai, A. Winkel, et al. 2019. "Commensal and Pathogenic Biofilms Differently Modulate Peri-Implant Oral Mucosa in an Organotypic Model." *Cellular Microbiology* 21, no. 10: e13078. <https://doi.org/10.1111/cmi.13078>.
- Kommerein, N., S. N. Stumpp, M. Musken, et al. 2017. "An Oral Multispecies Biofilm Model for High Content Screening Applications." *PLoS One* 12, no. 3: e0173973. <https://doi.org/10.1371/journal.pone.0173973>.
- Kotsakis, G. A., C. Lan, J. Barbosa, et al. 2016. "Antimicrobial Agents Used in the Treatment of Peri-Implantitis Alter the Physicochemistry and Cytocompatibility of Titanium Surfaces." *Journal of Periodontology* 87, no. 7: 809–819. <https://doi.org/10.1902/jop.2016.150684>.
- Kozlovsky, A., Z. Artzi, O. Moses, N. Kamin-Belsky, and R. B. Greenstein. 2006. "Interaction of Chlorhexidine With Smooth and Rough Types of Titanium Surfaces." *Journal of Periodontology* 77, no. 7: 1194–1200. <https://doi.org/10.1902/jop.2006.050401>.
- Lee, T. H., C. C. Hu, S. S. Lee, M. Y. Chou, and Y. C. Chang. 2010. "Cytotoxicity of Chlorhexidine on Human Osteoblastic Cells Is Related to Intracellular Glutathione Levels." *International Endodontic Journal* 43, no. 5: 430–435. <https://doi.org/10.1111/j.1365-2591.2010.01700.x>.
- Leoni, L., and P. Landini. 2014. "Microbiological Methods for Target-Oriented Screening of Biofilm Inhibitors." *Methods in Molecular Biology* 1147: 175–186. https://doi.org/10.1007/978-1-4939-0467-9_12.
- Leung, K., J. Bi, G. Giannelis, G. Owen, and H. Larjava. 2022. "Decontamination of Multispecies Oral Biofilm From Rough Implant Surface by Airflow With Glycine." *Clinical and Experimental Dental Research* 8, no. 1: 322–328. <https://doi.org/10.1002/cre2.507>.
- Loesche, W. J. 1979. "Clinical and Microbiological Aspects of Chemotherapeutic Agents Used According to the Specific Plaque Hypothesis." *Journal of Dental Research* 58, no. 12: 2404–2412. <https://doi.org/10.1177/00220345790580120905>.
- Luengo, F., J. Sanz-Esporrin, F. Noguerol, I. Sanz-Martin, I. Sanz-Sanchez, and M. Sanz. 2022. "In Vitro Effect of Different Implant Decontamination Methods in Three Intraosseous Defect Configurations." *Clinical Oral Implants Research* 33, no. 11: 1087–1097. <https://doi.org/10.1111/clr.13991>.
- Machtei, E. E., G. Romanos, P. Kang, et al. 2021. "Repeated Delivery of Chlorhexidine Chips for the Treatment of Peri-Implantitis: A Multicenter, Randomized, Comparative Clinical Trial." *Journal of Periodontology* 92, no. 1: 11–20. <https://doi.org/10.1002/JPER.20-0353>.
- Maleki Dizaj, S., H. Shokrgozar, J. Yazdani, M. Y. Memar, S. Sharifi, and M. A. Ghavimi. 2022. "Antibacterial Effects of Curcumin Nanocrystals Against *Porphyromonas gingivalis* Isolated From Patients With Implant Failure." *Clinics and Practice* 12, no. 5: 809–817. <https://doi.org/10.3390/clinpract12050085>.
- Martinez-Hernandez, M., B. Reda, and M. Hannig. 2020. "Chlorhexidine Rinsing Inhibits Biofilm Formation and Causes Biofilm Disruption on Dental Enamel In Situ." *Clinical Oral Investigations* 24, no. 11: 3843–3853. <https://doi.org/10.1007/s00784-020-03250-3>.
- Mikolai, C., N. Kommerein, A. Ingendoh-Tsakmakidis, A. Winkel, C. S. Falk, and M. Stiesch. 2020. "Early Host-Microbe Interaction in a Peri-Implant Oral Mucosa-Biofilm Model." *Cellular Microbiology* 22, no. 8: e13209. <https://doi.org/10.1111/cmi.13209>.
- Mohn, D., M. Zehnder, W. J. Stark, and T. Imfeld. 2011. "Electrochemical Disinfection of Dental Implants—a Proof of Concept." *PLoS One* 6, no. 1: e16157. <https://doi.org/10.1371/journal.pone.0016157>.
- Monje, A., E. Amerio, J. K. Cha, et al. 2022. "Strategies for Implant Surface Decontamination in Peri-Implantitis Therapy." *International Journal of Oral & Maxillofacial Implants* 15, no. 3: 213–248.
- Murai, H., M. Kuboniwa, M. Kakiuchi, R. Matsumura, Y. Hirata, and A. Amano. 2024. "Curcumin Inhibits Growth of *Porphyromonas gingivalis* by Arrest of Bacterial Dipeptidyl Peptidase Activity." *Journal of Oral Microbiology* 16, no. 1: 2373040. <https://doi.org/10.1080/20002297.2024.2373040>.
- Padial-Molina, M., J. Lopez-Martinez, F. O'Valle, and P. Galindo-Moreno. 2016. "Microbial Profiles and Detection Techniques in Peri-Implant Diseases: A Systematic Review." *Journal of Oral & Maxillofacial Research* 7, no. 3: e10. <https://doi.org/10.5037/jomr.2016.7310>.
- Racic, M., M. G. Grusovin, and L. Canullo. 2016. "The Microbiologic Profile Associated With Peri-Implantitis in Humans: A Systematic Review." *International Journal of Oral & Maxillofacial Implants* 31, no. 2: 359–368. <https://doi.org/10.11607/jomi.4150>.
- Ramanauskaitė, A., F. Schwarz, E. A. Cafferata, and P. Sahrman. 2023. "Photo/Mechanical and Physical Implant Surface Decontamination Approaches in Conjunction With Surgical Peri-Implantitis Treatment: A Systematic Review." *Journal of Clinical Periodontology* 50, no. Suppl 26: 317–335. <https://doi.org/10.1111/jcpe.13783>.
- Rasband, W. S. 2012. "ImageJ: Image Processing and Analysis in Java." *Renvert, S., and I. Polyzois. 2018. "Treatment of Pathologic Peri-Implant Pockets." *Periodontology 2000* 76, no. 1: 180–190. <https://doi.org/10.1111/prd.12149>.*
- Ryu, H. S., Y. I. Kim, B. S. Lim, Y. J. Lim, and S. J. Ahn. 2015. "Chlorhexidine Uptake and Release From Modified Titanium Surfaces and Its Antimicrobial Activity." *Journal of Periodontology* 86, no. 11: 1268–1275. <https://doi.org/10.1902/jop.2015.150075>.
- Sahrman, P., S. Winkler, A. Gubler, and T. Attin. 2021. "Assessment of Implant Surface and Instrument Insert Changes due to Instrumentation With Different Tips for Ultrasonic-Driven Debridement." *BMC Oral Health* 21, no. 1: 25. <https://doi.org/10.1186/s12903-020-01384-0>.
- Sahrman, P., M. Zehnder, D. Mohn, A. Meier, T. Imfeld, and T. Thurnheer. 2014. "Effect of Low Direct Current on Anaerobic Multispecies Biofilm Adhering to a Titanium Implant Surface." *Clinical Implant Dentistry and Related Research* 16, no. 4: 552–556. <https://doi.org/10.1111/cid.12018>.
- Sakai, K., N. Koyama, T. Fukuda, Y. Mori, H. Onaka, and H. Tomoda. 2012. "Search Method for Inhibitors of Staphyloxanthin Production by Methicillin-Resistant *Staphylococcus aureus*." *Biological & Pharmaceutical Bulletin* 35, no. 1: 48–53. <https://doi.org/10.1248/bpb.35.48>.
- Sanz-Martin, I., K. Paeng, H. Park, J. K. Cha, U. W. Jung, and M. Sanz. 2021. "Significance of Implant Design on the Efficacy of Different Peri-Implantitis Decontamination Protocols." *Clinical Oral Investigations* 25, no. 6: 3589–3597. <https://doi.org/10.1007/s00784-020-03681-y>.
- Schlee, M., F. Rathe, U. Brodbeck, C. Ratka, P. Weigl, and H. Zipprich. 2019. "Treatment of Peri-Implantitis-Electrolytic Cleaning Versus Mechanical and Electrolytic Cleaning-A Randomized Controlled Clinical Trial-Six-Month Results." *Journal of Clinical Medicine* 8, no. 11: 909. <https://doi.org/10.3390/jcm8111909>.
- Schlee, M., H. L. Wang, T. Stumpf, U. Brodbeck, D. Bosshardt, and F. Rathe. 2021. "Treatment of Periimplantitis With Electrolytic Cleaning Versus Mechanical and Electrolytic Cleaning: 18-Month Results From a Randomized Controlled Clinical Trial." *Journal of Clinical Medicine* 10, no. 16: 475. <https://doi.org/10.3390/jcm10163475>.

Schneider, S., M. Rudolph, V. Bause, and A. Terfort. 2018. "Electrochemical Removal of Biofilms From Titanium Dental Implant Surfaces." *Bioelectrochemistry* 121: 84–94. <https://doi.org/10.1016/j.bioelechem.2018.01.008>.

Sekino, S., P. Ramberg, N. G. Uzel, S. Socransky, and J. Lindhe. 2003. "Effect of Various Chlorhexidine Regimens on Salivary Bacteria and de Novo Plaque Formation." *Journal of Clinical Periodontology* 30, no. 10: 919–925. <https://doi.org/10.1034/j.1600-051x.2003.00420.x>.

Steiger-Ronay, V., A. Merlini, D. B. Wiedemeier, P. R. Schmidlin, T. Attin, and P. Sahrman. 2017. "Location of Unaccessible Implant Surface Areas During Debridement in Simulated Peri-Implantitis Therapy." *BMC Oral Health* 17, no. 1: 137. <https://doi.org/10.1186/s12903-017-0428-8>.

Stein, J. M., G. Conrads, M. M. H. Abdelbary, et al. 2023. "Antimicrobial Efficiency and Cytocompatibility of Different Decontamination Methods on Titanium and Zirconium Surfaces." *Clinical Oral Implants Research* 34, no. 1: 20–32. <https://doi.org/10.1111/clr.14014>.

Stringer, C., T. Wang, M. Michaelos, and M. Pachitariu. 2021. "Cellpose: A Generalist Algorithm for Cellular Segmentation." *Nature Methods* 18, no. 1: 100–106. <https://doi.org/10.1038/s41592-020-01018-x>.

Tonon, C. C., B. Panariello, M. Chorilli, D. M. P. Spolidorio, and S. Duarte. 2022. "Effect of Curcumin-Loaded Photoactivatable Polymeric Nanoparticle on Peri-Implantitis-Related Biofilm." *Photodiagnosis and Photodynamic Therapy* 40: 103150. <https://doi.org/10.1016/j.pdpdt.2022.103150>.

Ungvari, K., I. K. Pelsoczi, B. Kormos, et al. 2010. "Effects on Titanium Implant Surfaces of Chemical Agents Used for the Treatment of Peri-Implantitis." *Journal of Biomedical Materials Research. Part B, Applied Biomaterials* 94, no. 1: 222–229. <https://doi.org/10.1002/jbm.b.31644>.

Virto, L., V. Odeh, E. Garcia-Quismondo, et al. 2023. "Electrochemical Decontamination of Titanium Dental Implants. An In Vitro Biofilm Model Study." *Clinical Oral Implants Research* 34, no. 5: 486–497. <https://doi.org/10.1111/clr.14055>.

Wang, Z., H. Deng, L. Chen, Y. Xiao, and F. Zhao. 2013. "In Situ Measurements of Dissolved Oxygen, pH and Redox Potential of Biocathode Microenvironments Using Microelectrodes." *Bioresource Technology* 132: 387–390. <https://doi.org/10.1016/j.biortech.2012.11.026>.

Wheelis, S. E., I. M. Gindri, P. Valderrama, T. G. Wilson Jr., J. Huang, and D. C. Rodrigues. 2016. "Effects of Decontamination Solutions on the Surface of Titanium: Investigation of Surface Morphology, Composition, and Roughness." *Clinical Oral Implants Research* 27, no. 3: 329–340. <https://doi.org/10.1111/clr.12545>.

Wilensky, A., L. Shapira, A. Limones, and C. Martin. 2023. "The Efficacy of Implant Surface Decontamination Using Chemicals During Surgical Treatment of Peri-Implantitis: A Systematic Review and Meta-Analysis." *Journal of Clinical Periodontology* 50, no. Suppl 26: 336–358. <https://doi.org/10.1111/jcpe.13794>.

Supporting Information

Additional supporting information can be found online in the Supporting Information section.